Simulation of a single polymer chain in solution by combining lattice Boltzmann and molecular dynamics

Patrick Ahlrichs and Burkhard Dünweg

Articles you may be interested in

Implicit and explicit solvent models for the simulation of a single polymer chain in solution: Lattice Boltzmann versus Brownian dynamics
J. Chem. Phys. **131**, 164114 (2009); 10.1063/1.3251771

Lattice-Boltzmann simulations of the dynamics of polymer solutions in periodic and confined geometries
J. Chem. Phys. **122**, 094902 (2005); 10.1063/1.1854151

Simulation of polymer–polymer interdiffusion using the dynamic lattice liquid model
J. Chem. Phys. **120**, 6306 (2004); 10.1063/1.1649313

Molecular dynamics simulations of dielectric relaxation of concentrated polymer solutions
J. Chem. Phys. **111**, 1325 (1999); 10.1063/1.479318

Polyisoprene local dynamics in solution: Comparison between molecular dynamics simulations and optimized Rouse–Zimm local dynamics
J. Chem. Phys. **108**, 1245 (1998); 10.1063/1.475486

Simulation of a single polymer chain in solution by combining lattice Boltzmann and molecular dynamics

Patrick Ahlrichs and Burkhard Dünweg[a)]
Max Planck Institute for Polymer Research, Ackermannweg 10, D-55128 Mainz, Germany

In this paper we establish a new efficient method for simulating polymer–solvent systems which combines a lattice Boltzmann approach for the fluid with a continuum molecular-dynamics (MD) model for the polymer chain. The two parts are coupled by a simple dissipative force while the system is driven by stochastic forces added to both the fluid and the polymer. Extensive tests of the new method for the case of a single polymer chain in a solvent are performed. The dynamic and static scaling properties predicted by analytical theory are validated. In this context, the influence of the finite size of the simulation box is discussed. While usually the finite size corrections scale as L^{-1} (L denoting the linear dimension of the box), the decay rate of the Rouse modes is only subject to an L^{-3} finite size effect. Furthermore, the mapping to an existing MD simulation of the same system is done so that all physical input values for the new method can be derived from pure MD simulation. Both methods can thus be compared quantitatively, showing that the new method allows for much larger time steps. Comparison of the results for both methods indicates systematic deviations due to nonperfect match of the static chain conformations. © *1999 American Institute of Physics.* [S0021-9606(99)50840-4]

I. INTRODUCTION

The complexity and variety of soft condensed matter is largely due to the fact that length scales of different orders of magnitude are present.[1,2] When dealing with polymers in computer simulations, one therefore often intends to analyze the scaling behavior, where the nature of the underlying chemistry becomes unimportant.[1,3] When constructing models for these systems it is crucial to coarse–grain the details and to keep the relevant length scales in order to observe the phenomena one is interested in. Since bead–spring models in MD simulations are an appropriate means to yield the right universal laws, they have been widely used to simulate the scaling behavior of polymers and much progress has been made using these models.[4–9]

While in some systems, e.g., in highly concentrated solutions or in melts, the dynamic properties are not affected by the solvent—such that these can be simulated by conventional bead–spring models without explicitly taking into account the solvent—there are many phenomena in polymer science where the influence of the solvent on the polymer dynamics cannot be neglected. For example, in dilute or semidilute polymer solutions, the dynamical behavior is changed and even dominated by hydrodynamic interaction between different parts of the polymers. This eventually leads to a long–range interaction which is mediated by the solvent.[1,3] With this paper, we want to provide a new efficient method for the simulation of polymer systems where hydrodynamics plays a role. The idea is to focus on the really necessary parts only, i.e., the hydrodynamics of the solvent and the (Brownian) motion of the polymer chains, thereby trying to keep the computational costs at a minimum.

Our test case is the dynamics of a single chain in a solvent. This problem has continuously attracted the attention of MD researchers,[7–9] mainly because existing analytical theories[10–12] rely on uncontrollable assumptions that can be tested using computer simulations.

Simulating such systems by MD is only possible if one introduces explicit solvent particles. Hence one has to face the problem that almost all CPU time goes into the propagation of the solvent particles, while one is mainly interested in the chain properties. However, there are also other computational methods than MD available for soft condensed matter systems where hydrodynamics is important, not only in the field of polymers but for example also in colloidal suspensions. These include Brownian dynamics simulations,[13–16] and dissipative particle dynamics (DPD).[17–23] Both of them have inherent strengths, but also some disadvantages: The first technique must face the problem that the algorithm scales as the cube of the number of particles, and the latter (like MD) simulates the solvent particles explicitly, leading to simulations of several thousand particles even for a single chain of, say, 30 monomers. Compared to MD, DPD has the advantage of much larger time steps, mainly because of the use of very soft potentials.[19] A lot of progress in the theoretical framework of the method has been achieved,[20–22] but some practical problems remain, like the time step dependent temperature and the small Schmidt number.[19] Recently, however, some effort has been made to fill this gap.[23]

In this paper we use a recently proposed method[24] that couples a lattice Boltzmann approach for the fluid to bead–spring polymer chains. The lattice Boltzmann method (LBM)[25,26] was developed to simulate hydrodynamics on a grid. The LBM was shown to be an effective and fast method for simulating fluid flows, comparable to finite-difference[27]

[a)]Electronic mail: duenweg@mpip-mainz.mpg.de

or spectral methods.[28] Ladd applied the LBM successfully to colloidal systems:[27,29] The colloidal particles are simulated as hard spheres by using stick boundary conditions. This leads to a very efficient algorithm: Its CPU cost scales linearly with the number of particles, and it uses a ''minimal'' model to simulate the fluid. Besides, Ladd also showed[29] that fluctuations can be incorporated into the LBM in the spirit of Landau–Lifshitz fluctuating hydrodynamics,[30] which is essential if one wants to investigate Brownian motion.

Now one might think of a direct application of Ladd's method to polymer–solvent systems. However, using hard spheres to model the monomers is not necessary here, as rotational degrees of freedom as well as stick boundary conditions are not relevant: On the large length and time scales we are interested in, like the radius of gyration and the Zimm time of the polymer, it is sufficient that hydrodynamic interaction has evolved. The ''microscopic details'' of the coupling should then not play a role. In this spirit, we couple the LBM to bead-spring polymer chains by a simple friction ansatz, thereby treating the monomers as point particles for the fluid. We will show that this ansatz is sufficient to simulate both the static and dynamic scaling behavior of the polymer. The simulation of the fluid by LBM rather than explicit particles and the simple friction ansatz lead to a large speedup in computer time of about a factor of 20 when compared to pure MD, or even more if one is willing to be satisfied with less accurate data.

Additionally, we map our method to a pure MD simulation, i.e., we show how to determine all physical input values from the results of MD, allowing us to compare our results to an existing MD simulation with explicit solvent particles.[7] In other words, the fluid in the new method can be viewed as a coarse–grained MD fluid, and there exists a well–defined procedure for how to do the coarse–graining. Of course, in using such a mesoscopic approach it is no longer possible to include detailed chemistry like in atomistic MD simulations. This is, however, a quite common feature of mesoscopic simulation methods; DPD simulations do not include atomistic details either.

The remainder of this article is organized as follows: We outline the method in Sec. II, and present the numerical results in Sec. III, which are compared to pure MD in Sec. IV. In Sec. V we conclude with some final remarks and an outlook to further studies.

II. THE SIMULATION METHOD

A. The lattice Boltzmann method for the solvent

The lattice Boltzmann method is a discrete formulation of the Boltzmann equation on a lattice, leading to the Navier–Stokes equations in the incompressible limit by means of a Chapman–Enskog expansion.[25,26] It has been successfully applied to a variety of fluid flow problems, and it is especially well–suited for complex fluids because of the possibility of straightforward implementation of complex boundaries. The central quantity of the algorithm is $n_i(\mathbf{r},t)$, the number of particles in a volume a^3 at the grid point $\mathbf{r}$ at time t, which have the velocity $\mathbf{c}_i(a/\tau)$ ($i=1,...,b$), where a is the lattice spacing, τ the time step and $\mathbf{c}_i$ a vector leading

to the ith neighbor on a grid with unit lattice constant. The evolution equation for $n_i(\mathbf{r},t)$ is the lattice Boltzmann equation

$$n_i(\mathbf{r}+\mathbf{c}_i a,t+\tau)=n_i(\mathbf{r},t)+\sum_{j=1}^{b} L_{ij}(n_j(\mathbf{r},t)-n_j^{\mathrm{eq}}(\rho,\mathbf{u})). \quad (1)$$

The last term expresses the relaxation of n_i towards a local pseudo–equilibrium. The constant matrix L_{ij} can be interpreted as the scattering between particle population i and j. The well–known Bhatnagar–Gross–Krook (BGK) collision operator,[31] which is often used for both the discretized as well as the continuum Boltzmann equation, is the special case of a diagonal L_{ij}. Here, however, we use the more general form, and determine the structure of the matrix from physical and numerical arguments, as outlined in Ref. 29; the explicit form is actually not necessary for the implementation.

The local pseudo–equilibrium distribution $n_i^{\mathrm{eq}}(\rho,\mathbf{u})$ depends on the density $\rho(\mathbf{r},t)=\Sigma_i n_i(\mathbf{r},t)\mu/a^3$ and fluid current $\mathbf{j}(\mathbf{r},t)\equiv\rho\mathbf{u}=\Sigma_i n_i(\mathbf{r},t)\mathbf{c}_i\mu/(\tau a^2)$ only. Here, μ is the mass of a fluid particle. The usual functional form for $n_i^{\mathrm{eq}}(\rho,\mathbf{u})$ is assumed[26]

$$n_i^{\mathrm{eq}}(\rho,\mathbf{u})=\rho(A_q+B_q(\mathbf{c}_i\cdot\mathbf{u})+C_q u^2+D_q(\mathbf{c}_i\cdot\mathbf{u})^2). \quad (2)$$

The coefficients A_q, B_q, C_q, and D_q (which depend on the sublattice q, i.e., the magnitude of $\mathbf{c}_i$) are determined to reproduce the correct macroscopic hydrodynamic behavior. Note that this is contrary to continuum kinetic theory, where the Maxwell–Boltzmann distribution is determined by entropy considerations and the Navier–Stokes equations follow naturally by the Chapman–Enskog expansion.[32,33] Hence it is called *pseudo*–equilibrium. Explicit values for the coefficients A_q,B_q,C_q, and D_q are known for different lattices.[34]

Here, we implement the 18–velocity model of Ref. 29, which corresponds to the D3Q18 model in the nomenclature of Ref. 34. The set of $\mathbf{c}_i$ consists of the 6 nearest and 12 next-nearest neighbors on a simple cubic lattice. Via a Chapman–Enskog expansion one can show that this model leads to the Navier–Stokes equations in the limit of small Knudsen and Mach numbers,[25] and derive a relation between the kinematic viscosity ν and the nontrivial eigenvalue λ of L_{ij} belonging to the eigenvector $c_{i\alpha}c_{i\beta}$, ($\alpha,\beta=x,y,z,\alpha\neq\beta$),[34]

$$\nu=-\frac{1}{6}\left(\frac{2}{\lambda}+1\right)\frac{a^2}{\tau}. \quad (3)$$

In this paper, we always deal with low Reynolds number flow, hence the linearized Navier–Stokes equations are sufficient. For this reason, we neglect the nonlinear term in the equilibrium distribution (2), i.e., we effectively set $C_q=D_q=0$, thus obtaining a simpler and faster algorithm.[29]

Fluctuations can be incorporated into the lattice Boltzmann method.[29] The central idea is to add fluctuations to the fluxes of the conserved variables, i.e., the stress tensor, and not to the hydrodynamic fields ρ and $\mathbf{j}$. In this way, local mass and momentum conservation can be guaranteed.[30] The fluctuating lattice Boltzmann equation reads

$$n_i(\mathbf{r}+\mathbf{c}_i a,t+\tau)=n_i(\mathbf{r},t)+\sum_{j=1}^{b}L_{ij}(n_j(\mathbf{r},t)-n_j^{\text{eq}}(\rho,\mathbf{u}))$$

$$+n_i'(\mathbf{r},t), \tag{4}$$

with the stochastic term

$$n_i'(\mathbf{r},t)=-D_q\sum_{\alpha\beta}\sigma_{\alpha\beta}'c_{i\alpha}c_{i\beta}. \tag{5}$$

The random stress fluctuations $\sigma_{\alpha\beta}'$ are assumed to have white noise behavior

$$\langle\sigma_{\alpha\beta}'(\mathbf{r},t)\sigma_{\gamma\delta}'(\mathbf{r}',t')\rangle$$

$$=A\,\delta_{\mathbf{rr}'}\delta_{tt'}\big(\delta_{\alpha\gamma}\delta_{\beta\delta}+\delta_{\alpha\delta}\delta_{\beta\gamma}-\tfrac{2}{3}\delta_{\alpha\beta}\delta_{\gamma\delta}\big). \tag{6}$$

By solving the resulting discrete Langevin equation for the current one finds the fluctuation–dissipation relation[29] for this system; the noise strength A is given by

$$A=\frac{2\,\eta k_B T\lambda^2}{a^3\tau}, \tag{7}$$

where $\eta\equiv\nu\rho$ is the dynamic viscosity.

The LBM was tested extensively, compared to other Navier–Stokes solvers and found to have comparable speed and accuracy (see, for example, Refs. 25,27–29).

B. The bead-spring model for the polymer chain

The polymer model consists of repulsive Lennard–Jones monomers connected via finitely extendable nonlinear elastic springs (FENE potential)[6]

$$V_{\text{LJ}}=4\epsilon\left(\left(\frac{\sigma}{r}\right)^{12}-\left(\frac{\sigma}{r}\right)^6+\frac{1}{4}\right)\quad(r<2^{1/6}\sigma),$$

$$V_{\text{FENE}}=-\frac{kR_0^2}{2}\ln\left(1-\left(\frac{r}{R_0}\right)^2\right)\quad(r<R_0). \tag{8}$$

In order to model the excluded volume effect the Lennard–Jones potential acts between all monomers. As usual, the parameters ϵ, σ, and the mass m of the monomer define our unit system. Therefore we wrote the LBM in dimensional form in the last section, rather than using the usual dimensionless lattice units. The equations of motion resulting from these potentials are integrated using the velocity Verlet algorithm[35] with a time step Δt. Note that there is *a priori* no need to set $\Delta t=\tau$ and we will exploit this fact below.

The polymer model has been applied successfully to the simulation of many systems[4–6] including a single chain in explicit solvent,[7] so that we can compare chain properties in using these potentials.

C. Coupling of fluid and monomer

As mentioned above, for the length and time scales of the polymer chain, the ''microscopic'' details of the coupling should not play a role, as long as one assures that hydrodynamics evolves in the fluid on time scales faster than the diffusion time scale of the monomers. It is not necessary to resolve the shape of the monomer for the fluid. Thus, we can treat one monomer as a point particle. In analogy to the
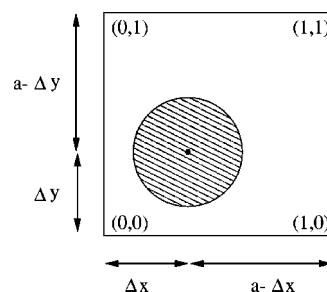

FIG. 1. Illustration of the quantities used for the coupling of monomer and fluid (in two dimensions). The figure shows a sketch of a monomer surrounded by the elementary cell of the four nearest neighbor grid points. a is the lattice constant.

Stokes formula for a sphere in a viscous fluid, we assume the force on the monomer exerted by the fluid to be proportional to the difference of the velocity of the monomer $\mathbf{V}$ and the fluid velocity $\mathbf{u}$ at the monomer's position

$$\mathbf{F}_{fl}=-\zeta[\mathbf{V}-\mathbf{u}(\mathbf{R},t)]. \tag{9}$$

Here, ζ is a proportionality coefficient which we will refer to as the ''bare'' friction coefficient. This ansatz has also been used in the simulation of sedimentation.[36]

Because the fluid velocity is only calculated at the discrete lattice sites in the simulation, one has to interpolate to get $\mathbf{u}(\mathbf{R},t)$ at the monomer's position. We implement a simple linear interpolation using the grid points on the elementary lattice cell containing the monomer: Denoting the relative position of the monomer in this cell by $(\Delta x,\Delta y,\Delta z)$, with the origin being at the lower left front edge (see Fig. 1), we can define

$$\delta_{(0,0,0)}=(1-\Delta x/a)(1-\Delta y/a)(1-\Delta z/a),$$

$$\delta_{(1,0,0)}=\Delta x/a\cdot(1-\Delta y/a)(1-\Delta z/a), \tag{10}$$

etc. The formula for the linear interpolation then reads

$$\mathbf{u}(\mathbf{R},t)=\sum_{\mathbf{r}\in\text{ng}}\delta_{\mathbf{r}}\mathbf{u}(\mathbf{r},t), \tag{11}$$

where ng denotes the grid points on the considered elementary lattice cell.

In order to conserve the total momentum of fluid and monomer we have to assign the opposite force to the fluid in that cell. Note that then the interaction is purely local. In particular, the force density $-\mathbf{F}_{fl}/a^3$ which is to be given to the fluid leads to a momentum density transfer per MD time step Δt of

$$-\mathbf{F}_{fl}/a^3=\frac{\Delta\mathbf{j}}{\Delta t}=\sum_{i,\mathbf{r}\in\text{ng}}\Delta n_i(\mathbf{r},t)\mathbf{c}_i\frac{\mu}{a^2\tau\Delta t}. \tag{12}$$

The last equation has to be satisfied for the change in the number of particles Δn_i of the grid points on the elementary lattice cell in order to exchange the momentum density $\Delta\mathbf{j}$. Besides, one must also ensure mass conservation in the fluid,

$$\sum_{i,\mathbf{r}\in\text{ng}}\Delta n_i(\mathbf{r},t)=0. \tag{13}$$

The way how to calculate the corresponding Δn_i at the nearest grid points is not unique; one possibility was presented in Ref. 24. Here, we follow a different approach which seems slightly more natural: For given hydrodynamic fields $\rho(\mathbf{r},t)$ and $\mathbf{j}(\mathbf{r},t)$ at a certain grid point $\mathbf{r}$, the equilibrium distribution can be calculated according to Eq. (2). The change in the equilibrium distribution at the points $\mathbf{r} \in$ ng due to the presence of the monomer can therefore be determined: ρ stays constant (mass conservation), while $\mathbf{j} \to \mathbf{j} + \delta_{\mathbf{r}} \Delta \mathbf{j}$. Here $\delta_{\mathbf{r}}$ is the fraction (10) of the total $\Delta \mathbf{j}$ which is given to the specific grid point $\mathbf{r}$. Therefore, by requiring that $n_i - n_i^{eq}$ remains unchanged, we obtain

$$\Delta n_i(\mathbf{r}) = B_q \delta_{\mathbf{r}} \Delta \mathbf{j} \cdot \mathbf{c}_i, \tag{14}$$

where again the nonlinear part of Eq. (2) has been neglected, consistent with our overall procedure. More accurate algorithms (which would, however, be computationally more expensive) could be constructed, using the method proposed in Ref. 37; however, this is not necessary for our purposes: Our simple approach is consistent with locality of the interaction, plus momentum conservation and should, therefore, suffice to build up hydrodynamic interactions in the correct manner.

As we discussed in Ref. 24, one has to take care when adding stochastic terms to the system. Due to the dissipative nature of the coupling, it is necessary to incorporate fluctuations to both the fluid and the monomers, i.e., to the LBM like in Eq. (4), and to the monomers by extending Eq. (9) to

$$\mathbf{F}_{fl} = -\zeta[\mathbf{V} - \mathbf{u}(\mathbf{R},t)] + \mathbf{f}. \tag{15}$$

Here $\mathbf{f}$ is a stochastic force of zero mean and

$$\langle f_\alpha(t) f_\beta(t') \rangle = \delta(t-t') 2 \delta_{\alpha\beta} k_B T \zeta. \tag{16}$$

The momentum transfer to the fluid for the fluctuating case is calculated in the same way as described above without the fluctuations. For this reason, the total momentum of fluid and polymer is conserved locally also in the fluctuating case. One can show analytically that with this method the fluctuation–dissipation relation holds for the continuum limit of the model, where the coupling to the LBM fluid is replaced by the analogous coupling to a Navier–Stokes fluid with thermal fluctuations of the flow field. For the velocities of the monomers and the fluid flow velocity, the equilibrium distribution is then given by the Maxwell–Boltzmann distribution, while the conformational statistics of the chain is given by the Boltzmann distribution, i.e., governed by the intrachain potentials V_{LJ} and V_{FENE}, see Eq. (8). This should be contrasted with the MD case, where the potential due to the solvent particles has an additional influence. For the discrete case, one can check the fluctuation–dissipation relation by investigating the velocity relaxation of one (initially kicked) monomer in the fluid on the one hand, and the velocity autocorrelation, if fluctuations are added, on the other hand. The two quantities coincide for our model,[24] which is expected from linear response theory. It is also interesting to note that in the overdamped limit for the monomer motion, and the continuum limit for the fluid, our approach is identical to the Oono–Freed equations of motion,[38] which are commonly used in polymer solution theory.

The main justification of our approach relies on the fact that a hydrodynamic (Navier–Stokes) description of the fluid works down to very short (actually, surprisingly short) length and time scales. Therefore, one should expect that the flow around a monomer should be describable by the solution of the Navier–Stokes equation as soon as the distance is larger than a few lattice spacings. The same argument holds for the analogous MD system, where one expects Navier–Stokes behavior beyond a few particle diameters. Therefore, we may say that any two local couplings (for example, our LBM friction ansatz vs MD) are equivalent as soon as they produce the same long–range flow field. If this is the case, then the hydrodynamic interaction between two monomers (as long as they are not too close) will be identical, and the single-monomer mobilities will also match (note that for a particle which is pulled through the fluid at constant velocity by a constant force, the friction coefficient is determined by the energy dissipated in the surrounding flow field).

This latter property actually allows for an easy determination of the simulation parameter ζ, which we will now, for the sake of clarity, denote by the symbol ζ_{bare}. A heuristic procedure, which was followed in Ref. 24, is to vary this parameter in a set of simulations of a single monomer in solvent (which can be done very easily), and to measure the momomer diffusion coefficient D_0, until the latter has the desired value. If viscosity and fluid density match as well, then the long–range parts of the flow fields (beyond a few lattice spacings) must look the same. It should be noted that the Einstein relation $D_0 = k_B T/\zeta_{eff}$ thus defines an effective or renormalized friction coefficient, which differs from the original bare one, as it contains all the effects of hydrodynamic interaction. Since these tend to increase the mobility, one has $\zeta_{eff} < \zeta_{bare}$. More quantitatively, one can argue as follows: Let us consider a particle which is pulled through the solvent at constant velocity $\mathbf{V}$ by an external force $\mathbf{F}$. Then, rewriting Eq. (9), we find

$$\mathbf{V} = \frac{1}{\zeta_{bare}} \mathbf{F} + \mathbf{u}_{av}, \tag{17}$$

where $\mathbf{u}_{av}$ is the flow velocity averaged over the nearest lattice sites of the particle, as implemented by our interpolation procedure. However, to a good approximation, the flow field should be given by the Oseen tensor:

$$\mathbf{u} = \frac{1}{8\pi\eta r}(\mathbf{1} + \hat{\mathbf{r}} \otimes \hat{\mathbf{r}})\mathbf{F}, \tag{18}$$

where r is the distance from the particle. Hence the averaged flow field should—in our case of averaging roughly at a distance a from the particle—have the form

$$\mathbf{u}_{av} = \frac{1}{g\eta a}\mathbf{F}, \tag{19}$$

where g is an unknown numeric constant describing the details of the lattice geometry and of the averaging procedure. For example, doing the average over a sphere of radius d, one would directly obtain $\mathbf{u}_{av} = \mathbf{F}/(6\pi\eta d)$, from which one easily derives Stokes' law. Combining these results and using $\zeta_{eff}\mathbf{V} = \mathbf{F}$ one obtains

J. Chem. Phys., Vol. 111, No. 17, 1 November 1999
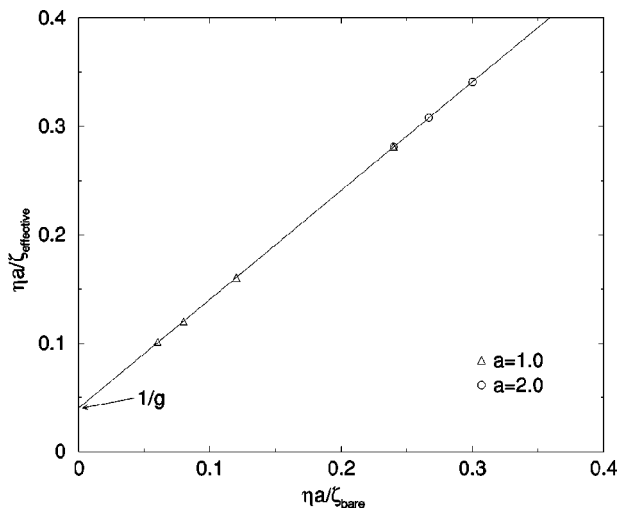
Simulation of a single polymer chain   8229

FIG. 2. Test of the predicted relation between bare and effective friction coefficient, Eq. (20). Grids of different lattice spacings were used as indicated in the figure.

$$\frac{1}{\zeta_{\mathrm{eff}}} = \frac{1}{\zeta_{\mathrm{bare}}} + \frac{1}{g \, \eta a}, \qquad (20)$$

i.e., the overall mobility is simply the sum of the bare mobility and a hydrodynamic, Stokes-type contribution, where the lattice discretization serves to provide an effective Stokes radius of the monomers. This relation has been tested by running several simulations at different bare couplings and different lattice constants; the agreement is remarkable, as seen from Fig. 2, where we plot $\eta a / \zeta_{\mathrm{eff}}$ as a function of $\eta a / \zeta_{\mathrm{bare}}$. The parameter g is thus found to have the value $g \approx 25$ for our method.

The lattice constant a hence appears not only as a parameter which controls how accurately the Navier–Stokes equation is solved (this is the usual case for Navier–Stokes equation solvers), but it is being assigned an additional meaning as an effective Stokes radius. For that reason, it cannot be varied arbitrarily, but only within limits: A too small lattice constant would result in an unphysically large particle mobility, even if ζ_{bare} is very large. This is quite different from conventional Navier–Stokes equation solving, where one obtains systematically better results when a is decreased, and can be viewed as the price which has to be paid for introducing the simple and computationally fast concept of a point particle, which is, however, strictly spoken, unphysical. It should be noted that ζ_{bare} controls the degree of coupling to the flow field: For small ζ_{bare}, one has $\zeta_{\mathrm{eff}} \approx \zeta_{\mathrm{bare}}$, while for large ζ_{bare} the Stokes contribution prevails, $\zeta_{\mathrm{eff}} \approx g \, \eta a$. It should have become clear that hence ζ_{bare} has no real physical meaning whatsoever; it is really the effective friction which matters for the coupling.

III. SINGLE CHAIN SIMULATION

A. Input parameters

The present model is intended to represent the same physical situation as an existing pure MD simulation.[7] We, therefore, choose the physical input values for the new method as obtained by the former (all values are given in the unit system specified in Sec. II B). The fluid is characterized by the temperature $k_B T = 1.2$, the density $\rho = 0.864$, and the kinematic viscosity $\nu = 2.8$. The parameter μ (the fluid particle mass) is unimportant; its value can be absorbed in a re-definition of the n_i. The lattice constant a of the grid is set to unity; this is roughly the same as the bond length of the polymer chain, and the interparticle distance of the MD fluid. As in the pure MD simulation, we study chains of length $N_{\mathrm{ch}} = 30, 40$, and 60. The corresponding grid sizes (which are important parameters, since they determine the hydrodynamic interaction of the chain with its periodic images, see Ref. 7) are $L = 18, 18$, and 22, respectively, which is roughly identical to the corresponding MD box sizes.

The parameters for the FENE potential are taken from the MD simulation as $R_0 = 2.0$ and $k = 7.0$. As already discussed in Sec. II C, this does, however, not assure that the static conformations are identical: In the MD case, there is also the influence of the solvent, which is absent in the present method. Actually, the data show a systematic deviation, which is however not very large (see Sec. III B).

The mass of the monomers was set to unity. This actually differs from the MD case where the monomer mass had been set to two. However, we also used a monomer of mass one in order to determine the ''bare'' friction coefficient ζ_{bare}, using the procedure outlined at the end of Sec. II C, such that we found $\zeta_{\mathrm{bare}} = 20.8$ from the requirement that the monomer diffusion coefficient has the value known from MD, $D_0 = 0.076$. Had we used a monomer of different mass, we would also have obtained a slightly different value for ζ_{bare} [these are very small effects, beyond what the simple picture which underlies Eq. (20) can capture]. Since however on the time scale of Brownian motion it is only the parameter $\zeta_{\mathrm{eff}} = k_B T / D_0$ which matters, we expect an influence of the mass parameter only for short times, where the dynamics differs from MD behavior anyways.

It remains to specify the time steps Δt and τ. A choice of $\Delta t = 0.01$ is optimal for the MD part.[6] Concerning the LBM time step τ it is desirable to make it as large as possible because the fluid calculation is the CPU intensive part of the method. Test simulations showed the limiting factor to be that n_i is getting negative for too large time steps due to increasing fluctuations, in particular near the monomers. This situation, however, can always happen, although with decreasing probability for smaller time steps. We found that using a time step of $\tau = 0.05$ only approximately each 10^4th random number one n_i became negative, while for $\tau = 0.01$ such a case never occurred during the observation time. We decided to generate new random numbers in such rare cases, which of course slightly changes the distribution of the simulated noise, but is justified if the probability for negative n_i's is low enough. We ran the simulations at $\tau = 0.05$ and also did a simulation for the smallest system ($N_{\mathrm{ch}} = 30$, $L = 18$) using $\tau = 0.01$ in order to check the results.

Furthermore, we should comment in some more detail on the lattice constant a. The choice $a = 1$ seems intuitively reasonable, since this matches the bond length and the interparticle distance in the MD system. However, one would in principle like to make the lattice spacing as large as possible, since, for constant overall volume, the computational effort

TABLE I. Single chain properties.

Chain length	30	30	40	60
LB time step τ	0.05	0.01	0.05	0.05
exponent ν	0.621 ± 0.004	0.620 ± 0.002	0.637 ± 0.002	0.637 ± 0.002
$\langle R_e^2 \rangle$	94 ± 5	90 ± 4	134 ± 4	217 ± 10
$\langle R_g^2 \rangle$	14.3 ± 0.5	13.9 ± 0.4	20.6 ± 0.3	33.5 ± 0.9
$\left\langle \dfrac{1}{R_H} \right\rangle_\infty$	0.299 ± 0.005	0.300 ± 0.005	0.261 ± 0.005	0.215 ± 0.004
$\left\langle \dfrac{1}{R_H} \right\rangle_L^a$	0.1512	0.1525	0.1179	0.0986
k_BT	1.139 ± 0.003	1.2056 ± 0.003	1.139 ± 0.003	1.139 ± 0.003
g_3-exp.[b]	0.9951 ± 0.0004	1.009 ± 0.0002	1.0001 ± 0.0001	1.006 ± 0.003
g_1-exp.[b]	0.6415 ± 0.001	0.6747 ± 0.001	0.6630 ± 0.0006	0.6704 ± 0.002
D_{CM}	6.533×10^{-3} $\pm1\times10^{-5}$	6.102×10^{-3} $\pm1\times10^{-5}$	4.860×10^{-3} $\pm2\times10^{-5}$	3.387×10^{-3} $\pm1\times10^{-5}$
$D_0{}^c$	0.081	0.062	0.076	0.054
τ_Z (estimate)	365	380	705	1650

[a]No error due to complicated calculation.
[b]Exponent obtained by fitting a power law in the sub-diffusive scaling regime $t\in[20:80]$.
[c]Calculated using Eq. 31.

scales as a^{-3}. For this reason, we also did a test run with $a=2$ for the $N_{ch}=30$ system, where we of course had re–adjusted the bare friction, see end of Sec. II C. It turned out that the decay of the dynamic structure factor looks quite similar. However, there are systematic discrepancies (see Sec. IV B), such that the gain in speed is paid for by a certain loss in accuracy. In what follows we will always refer to the case $a=1$, unless explicitly stated otherwise.

An important point concerning the comparison with analytical theory should be mentioned here. It is usually assumed in these theories that the time scale for the evolution of the hydrodynamic interaction is much smaller than the diffusion time scale of a monomer, i.e., the Schmidt number $Sc=(\nu/D_0)\gg1$. This parameter can be set arbitrarily in our method: ν is an input parameter and D_0 can be tuned by choosing ζ_{bare}. In our case, we have $Sc\approx32$.

B. Chain statics

The results for the chain lengths of $N_{ch}=30$, 40, and 60 are listed in Table I. The measurement of the chain's temperature provides a first consistency check of the algorithm. The values for $k_BT_{measured}\equiv[2/(3N_{ch})]E_{kin}$ show a discretization error of 5% for the large time step $\tau=0.05$. For the small time step $\tau=0.01$ the error decreases significantly.

The radius of gyration

$$\langle R_G^2 \rangle = \frac{1}{2N_{ch}^2}\sum_{ij}\langle r_{ij}^2 \rangle, \qquad (21)$$

with $r_{ij}=|\mathbf{r}_i-\mathbf{r}_j|$, and the end-to-end distance

$$\langle R_e^2 \rangle = \langle (\mathbf{r}_{N_{ch}}-\mathbf{r}_1)^2 \rangle \qquad (22)$$

are related to the number of monomers by the static exponent ν

$$\langle R_g^2 \rangle \propto \langle R_e^2 \rangle \propto N_{ch}^{2\nu}; \qquad (23)$$

for a self-avoiding walk $\nu\approx0.588$ from renormalization group theory methods and Monte Carlo simulation.[39] In principle, ν can be obtained from the scaling law (23); however, this would require simulations covering a wide range of N_{ch}. Hence, it is advantageous to use the static structure factor

$$S(k)=N_{ch}^{-1}\sum_{ij}\langle\exp(i\mathbf{k}\cdot\mathbf{r}_{ij})\rangle=N_{ch}^{-1}\sum_{ij}\left\langle\frac{\sin(kr_{ij})}{kr_{ij}}\right\rangle, \qquad (24)$$

which probes different length scales even for a single polymer. In the scaling regime $R_g^{-1}\ll k\ll a_0^{-1}$ (a_0 being a microscopic length of the order of the bond length) the relation

$$S(k)\propto k^{-1/\nu}, \qquad (25)$$

holds.[3] By fitting a power law to our data (see Fig. 3) we get the values for ν of Table I which are about 6% higher than the asymptotically correct value, resulting from the finite
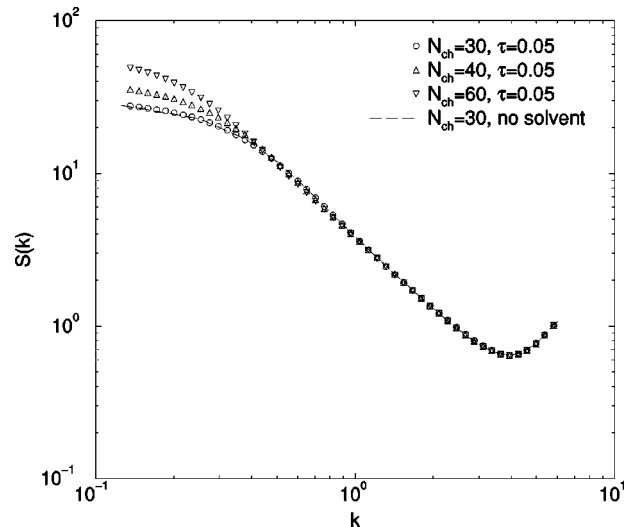

FIG. 3. The static structure factor of the chains.

chain length. In Fig. 3 we also include data which have been generated from a simulation of a single chain *without* surrounding LBM fluid. The conformations must be the same, i.e., the structure factors must coincide (up to discretization errors, which may look somewhat different for the chain coupled to the LBM fluid). As is seen from the figure, the agreement is very good, i.e., the method is validated to produce correct static conformations.

The hydrodynamic radius

$$\left\langle \frac{1}{R_H} \right\rangle_\infty = \frac{1}{N_{ch}^2} \sum_{i \neq j} \left\langle \frac{1}{r_{ij}} \right\rangle, \tag{26}$$

is an interesting quantity because the Kirkwood prediction for the diffusion of the chain's center of mass[10,11]

$$D_{CM} = \frac{D_0}{N_{ch}} + \frac{k_B T}{6 \pi \eta} \left\langle \frac{1}{R_H} \right\rangle_\infty, \tag{27}$$

depends on it. This formula, however, is only correct for a single chain in an infinite medium. In a finite box one has to take into account the hydrodynamic interaction with the periodic images. This will eventually lead to a finite-size corrected hydrodynamic radius. Quite generally, one must expect a finite size effect of order L^{-1} for every dynamic quantity, corresponding to the slow r^{-1} decay of hydrodynamic interactions. A detailed description can be found in Refs. 7 and 40, so that we can restrict ourselves to the essential points. Within the Oseen approximation, the diffusion tensor is given by

$$\mathbf{D}_{ij} \equiv \mathbf{D}(\mathbf{r}_{ij}) = \frac{k_B T}{\eta L^3} \sum_{\mathbf{k} \neq 0} \frac{\mathbf{1} - \hat{\mathbf{k}} \otimes \hat{\mathbf{k}}}{k^2} \exp(i\mathbf{k} \cdot \mathbf{r}_{ij}) \tag{28}$$

for $i \neq j$, where $\mathbf{k} = 2\pi \mathbf{n}/L$ ($\mathbf{n}$ being a vector of integers) runs over the reciprocal lattice vectors and $\hat{\mathbf{k}}$ is a unit vector in the direction of $\mathbf{k}$. For $i = j$, one has the monomeric diffusion coefficient D_0, plus the contribution due to the hydrodynamic interaction of that bead with its own periodic images,

$$\mathbf{D}_{ii} = D_0 \mathbf{1} + \lim_{\mathbf{r} \to 0} \left(\mathbf{D}(\mathbf{r}) - \frac{k_B T}{8 \pi \eta r} (\mathbf{1} + \hat{\mathbf{r}} \otimes \hat{\mathbf{r}}) \right). \tag{29}$$

The last two expressions can be calculated efficiently using the Ewald summation technique. The center of mass diffusion constant is given by

$$D_{CM} = \frac{1}{N_{ch}^2} \sum_{ij} \frac{1}{3} \mathrm{Tr} \langle \mathbf{D}_{ij} \rangle. \tag{30}$$

Inserting Eqs. (28) and (29) one obtains[7]

$$D_{CM,L} = \frac{D_0}{N_{ch}} - \frac{2.837 \, k_B T}{6 \pi \eta L N_{ch}} + \frac{1}{3 N_{ch}^2} \sum_{i \neq j} \mathrm{Tr} \langle \mathbf{D}_{ij} \rangle, \tag{31}$$

which defines, by comparison with the Kirkwood formula (27), a finite size corrected hydrodynamic radius

$$D_{CM,L} \equiv \frac{D_0}{N_{ch}} + \frac{k_B T}{6 \pi \eta} \left\langle \frac{1}{R_H} \right\rangle_L. \tag{32}$$

R_H is thus effectively increased by the periodic images. For our box sizes, the discrepancy between $\langle R_H^{-1} \rangle_L$ and $\langle R_H^{-1} \rangle_\infty$
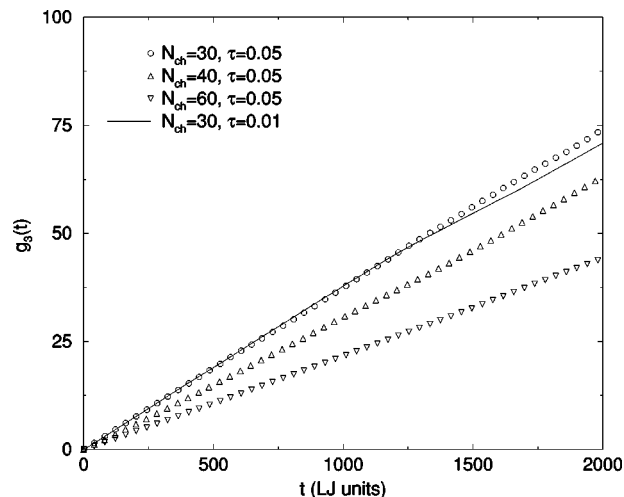

FIG. 4. The mean-square displacement of the chain's center of mass.

amounts to approximately a factor of 2 (cf. Table I). This is in agreement with the corrections found in Ref. 7.

C. Chain dynamics

The dynamic scaling picture for Zimm dynamics[3] starts from the prediction $D_{CM} \propto R_g^{-1}$ [cf. Eq. (27)]. The Zimm time τ_Z, i.e., the longest relaxation time of the chain, is given by the condition that the chain has moved its own size during τ_Z, or $D_{CM} \tau_Z \propto R_g^2$, implying $\tau_Z \propto R_g^3$, which defines the dynamic exponent $z = 3$. This exponent then quite generally relates times to corresponding lengths, such that, for example, the mean square displacement of a monomer on time scales below τ_Z, but above the microscopic time scales τ_0, should be proportional to $t^{2/z} = t^{2/3}$. For a chain without hydrodynamic interaction (Rouse model), where $D_{CM} \propto N_{ch}^{-1}$, one finds $z = 2 + 1/\nu$ from analogous considerations.

Figure 4 shows the mean-square displacement of the chain's center of mass

$$g_3(t) = \langle (\mathbf{R}_{CM}(t_0 + t) - \mathbf{R}_{CM}(t_0))^2 \rangle. \tag{33}$$

By fitting a power law we obtain the exponents and the diffusion constants shown in Table I. Obviously, the exponents support the prediction of simple diffusive behavior (t^1). One would expect theoretically that two diffusive regimes exist, both exhibiting t^1 behavior but different prefactors, with a smooth crossover around the Zimm time. The accuracy of the data does not allow to support this crossover, which is not surprising as the short-time and long-time diffusion constant are expected to be rather close to each other.[16,41,42] In principle, the scaling behavior of D_{CM} provides a test of the Zimm prediction $D_{CM} \propto N_{ch}^{-\nu}$. But there are large corrections to scaling due to finite chain length and bead size effects.[7,43] Therefore, it is more useful to analyze the nonasymptotic relation (31) by comparing the values for D_0 that can be obtained from Eq. (31), where finite chain length and finite box size are taken into account, with the input value of $D_0 = 0.076$. The values are also listed in Table I showing quite reasonable agreement. Without the finite size corrections, the agreement is unacceptable, such that a negative value for D_0 would be obtained.
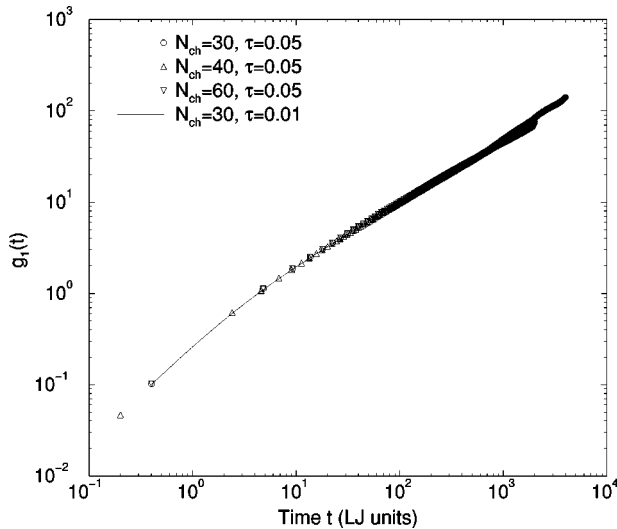
FIG. 5. The mean-square displacement of the central monomer.

The mean-square displacement of a single monomer i (which should only be evaluated for monomers near the center of the chain to eliminate end effects)

$$g_1(t) = \langle (\mathbf{r}_i(t+t_0) - \mathbf{r}_i(t_0))^2 \rangle, \qquad (34)$$

is plotted in Fig. 5. In the time regime below the Zimm time and above the ballistic regime, the scaling behavior $g_1(t) \propto t^{2/3}$ is predicted. The corresponding fit to our data yields the exponents of Table I. The values obviously favor the Zimm model compared to the Rouse model, which predicts $g_1(t) \propto t^{2/z} = t^{0.54}$.

The Zimm time can be estimated from the mean-square displacement of a monomer in the center of mass system

$$g_2(t) = \langle ([\mathbf{r}_i(t+t_0) - \mathbf{R}_{CM}(t+t_0)] - [\mathbf{r}_i(t_0)$$
$$- \mathbf{R}_{CM}(t_0)])^2 \rangle, \qquad (35)$$

which is depicted in Fig. 6. Theoretically, a crossover to a plateau should evolve at the Zimm time. However, the cross-
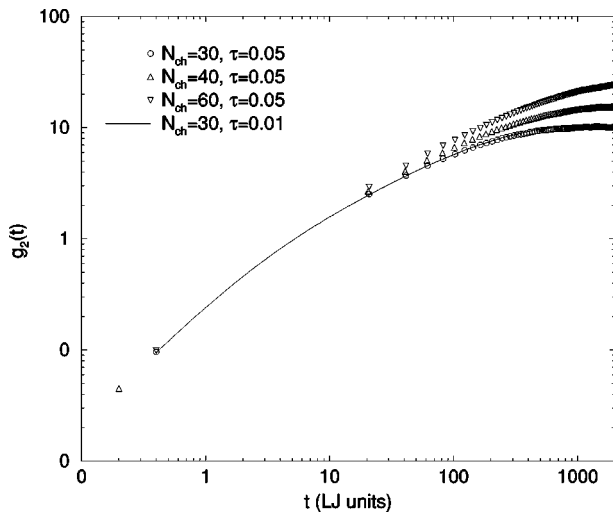

FIG. 6. The mean-square displacement of the central monomer in the chain's center-of-mass system.

over is quite extended in our simulation, making it difficult to extract a specific time for it. We therefore estimate the Zimm time from

$$\tau_Z = \frac{\langle R_g^2 \rangle}{6D_{CM}}, \qquad (36)$$

which yields the values shown in Table I.

It is interesting to perform a Rouse mode analysis. For this purpose one defines the Rouse modes as[44]

$$\mathbf{X}_p = N_{ch}^{-1} \sum_{n=1}^{N_{ch}} \mathbf{r}_n \cos\left[\frac{p\pi}{N_{ch}} \left(n - \frac{1}{2} \right) \right]. \qquad (37)$$

It is well known that these modes are the (independent) eigenmodes of the random walk Rouse model.[3] However, for reasons of translational symmetry along the chain, one must expect that the cross correlation $\langle \mathbf{X}_p(t+t_0)\mathbf{X}_q(t_0) \rangle (p \neq q)$ is at any rate quite weak, regardless of chain statistics and dynamics, such that the modes can be viewed as independent modes even beyond the random walk Rouse case. For a ring polymer, this can be shown rigorously, since in this case there is strict invariance under the transformation $n \to n+1$, such that the Rouse modes (which are then defined with an $\exp(ip\pi n/N_{ch})$ factor) are eigenfunctions under this transformation. Hence, if end effects are not too strong, one should also expect for our case an independence of the Rouse modes. Indeed, within the accuracy of our data, the cross correlation terms are zero.

Furthermore, within the approximations of the Zimm model, the autocorrelation function of the modes should decay exponentially[3]

$$\frac{\langle \mathbf{X}_p(t+t_0)\mathbf{X}_p(t_0) \rangle}{\langle \mathbf{X}_p^2 \rangle} = \exp(-t/\tau_p). \qquad (38)$$

In Fig. 7, we therefore plot, for $p \geq 1$, the normalized autocorrelation function semilogarithmically as a function of properly scaled time. Firstly, we estimate τ_p via the initial decay rate

$$\tau_p^{-1} = \Gamma_p = -\frac{d}{dt} \left(\frac{\langle \mathbf{X}_p(t)\mathbf{X}_p(0) \rangle}{\langle \mathbf{X}_p^2 \rangle} \right)\Bigg|_{t=0}, \qquad (39)$$

which can, within the framework of Kirkwood–Zimm theory, be calculated in terms of purely static averages, i.e., from the chain conformations in combination with a model diffusion tensor, for which we use Eqs. (28) and (29). The details of this approach are described in the Appendix. Interestingly, it turns out that this quantity is only subject to an L^{-3} finite size effect (which we neglect), in contrast to the usual L^{-1} behavior. This result holds beyond the various approximations of the Appendix; our interpretation is that any contribution of global center-of-mass motion of the chain is being subtracted, such that the leading-order hydrodynamic interaction with the periodic images cancels out, and only a dipole-type interaction remains. In the upper part of Fig. 7, we thus plot the autocorrelation as a function of $\Gamma_p t$, where Γ_p was calculated directly from the simulated chain conformations, in combination with the Oseen tensor. It is seen that the Oseen formula describes the decay quite
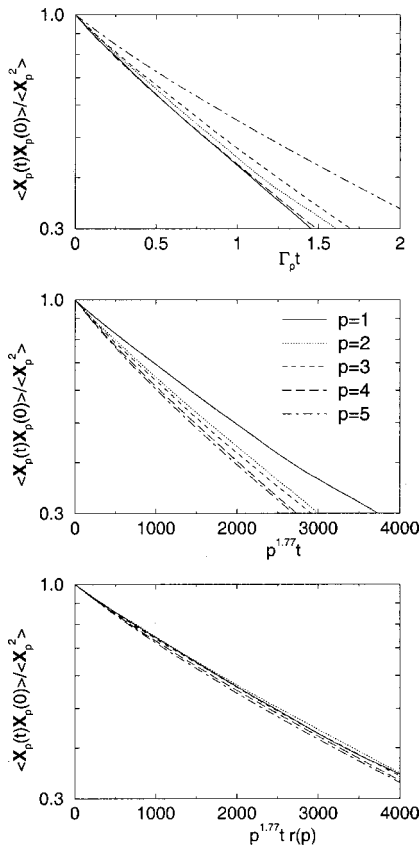
FIG. 7. Normalized autocorrelation function of the Rouse mode $\mathbf{X}_p$ for different p, for the longest simulated chain $N_{ch}=60$. The upper part of the figure uses $\Gamma_p t$ as scaling argument, where Γ_p was calculated directly from the chain conformations. The middle part uses $p^{z\nu}t$, where naive dynamic scaling has been applied, while the lower part also takes the correction factor $r(p)$ (see Appendix) into account. The meaning of symbols is the same for all three parts (see middle part).

well; however, the data collapse is not particularly good. There is also some curvature, indicating a nonexponential decay. The middle part of the figure then uses the scaling argument $p^{z\nu}t$. This p-dependence results from the calculation of Γ_p, where instead of the actual chain conformations asymptotic self–avoiding walk statistics is employed (see the Appendix), as the leading power law. This corresponds to simple dynamic scaling, which views the pth mode as equivalent to a chain of length N_{ch}/p, such that $\tau_p \propto (N_{ch}/p)^{\nu z}$. However, the more detailed calculation of the Appendix yields an additional weak p–dependence, i.e., a correction factor $r(p)$, whose presence indicates, in our opinion, that the simple picture of subchains of length N_{ch}/p is not fully justified. Taking this correction into account, we obtain a very nice data collapse (see lower part of Fig. 7). This is quite remarkable; one would of course expect the best data collapse for the uppermost part which involves the smallest number of approximations. It seems that there are various errors involved which somehow happen to cancel out. As far as the absolute value of the decay rate is concerned we find reasonable agreement: While the lower part of Fig. 7 shows a decay rate of roughly $3\times10^{-4}p^{3\nu}r(p)$, Eq. (A21) predicts a decay rate of order $5.4\times10^{-4}p^{3\nu}r(p)$

where we have for simplicity used the random walk value for the constant A, and $b^3=2.0$ (extracted from the results for R_e^2 via $R_e^2=b^2N^{2\nu}$).

The dynamic structure factor

$$S(k,t)=\frac{1}{N_{ch}}\sum_{ij}\langle\exp(i\mathbf{k}\cdot[\mathbf{r}_i(t)-\mathbf{r}_j(0)])\rangle, \quad (40)$$

is predicted[3] to exhibit the scaling behavior

$$S(k,t)=S(k,0)f(k^z t), \quad (41)$$

if both wave number and time are in the scaling regime, i.e., $R_g^{-1}\ll k\ll a_0^{-1}$ and $\tau_0\ll t\ll\tau_Z$. It is even possible to calculate explicit formulas (rigorously for the random walk Rouse model and using the linearization approximation in the Zimm case),[3,45,46] which suggest that there is an exponential dependency on $(k^z t)^{2/z}$ for $\Gamma_k t\gg1$, where Γ_k is the (k-dependent) decay rate. Hence a plot of $S(k,t)k^{1/\nu}$ against $(k^z t)^{2/z}$ should—for the correct model—collapse to a straight line in a log-linear representation. For $N_{ch}=60$, the results are shown in Fig. 8 (the plots for the other chain lengths look quite similar). The data were restricted to the scaling regime $20\leq t\leq80$ and $0.7\leq k\leq2$. These ranges were obtained from the single–monomer mean square displacement, Fig. 5, and from the static structure factor, Fig. 3, respectively. Values of $S(k,t)$ below 0.01 were discarded, for reasons of statistical accuracy. It is clearly visible that the simulation shows Zimm rather than Rouse behavior. A dynamic exponent of $z=2.8$ yields the best data collapse. Such an effective value, which is, due to corrections to scaling, somewhat smaller than the correct asymptotic one, is quite usually observed, not only in simulations,[8] but also in experiments.[1]

Concerning finite size effects, one has for a finite box size $S=S(k,t,L)$, and scaling is corrupted by the second length L in the problem. The influence can be estimated, in close analogy to the procedure presented in the Appendix, by studying the Akcasu formula for the k–dependent diffusion coefficient,[46,47]

$$D(k,L)=\frac{\sum_{ij}\langle\hat{\mathbf{k}}\cdot\mathbf{D}_{ij}\cdot\hat{\mathbf{k}}\exp(i\mathbf{k}\mathbf{r}_{ij})\rangle}{\sum_{ij}\langle\exp(i\mathbf{k}\mathbf{r}_{ij})\rangle}, \quad (42)$$

which is L-dependent because of the finite size form (28) of $\mathbf{D}_{ij}$. $D(k,L)$ is related to the initial slope of the dynamic structure factor via

$$D(k,L)=-\lim_{t\to0}\frac{1}{k^2t}\ln\left(\frac{S(k,t,L)}{S(k,0,L)}\right). \quad (43)$$

We do not present the details of our semiquantitative analysis here since they have been outlined in Ref. 7 already. The result is a k–independent correction term of order L^{-1} (note that $S(k,t)$ does contain the overall chain motion, for every wave number). As the leading-order ($L=\infty$) term is proportional to k in the scaling regime, the conclusion is that scaling is corrupted, but the relative contribution of the finite size correction gets weaker with increasing k. For the $k\to0$ limit finite size corrections amount to roughly 100%, as has been shown by the calculations for the hydrodynamic radius in Sec. III B. In the scaling regime the corrections are much
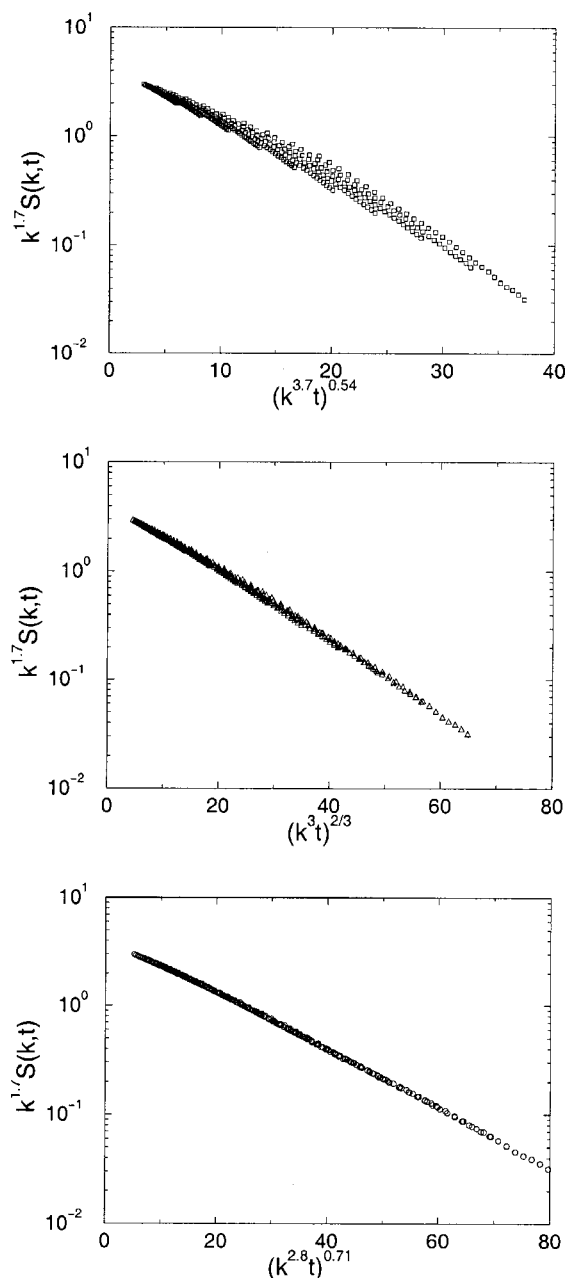
FIG. 8. Scaling plot of the dynamic structure factor for $N_{ch}=60$, for Rouse scaling ($z=3.7$), asymptotic Zimm scaling ($z=3$), and $z=2.8$, which produces the best collapse.

smaller, because it is closer to the $kL\rightarrow\infty$ limit. This is, in our opinion, the main reason why the data collapse works so nicely.

IV. COMPARISON TO THE CORRESPONDING MD SYSTEM

A. Efficiency

Since the system is highly dilute, the CPU cost for the MD part for the polymer chain is negligible, and the lattice Boltzmann part uses up practically all computational resources. It should be noted that this part can be optimized by choosing appropriate simulation parameters; our choice ($a=1$, $\tau=0.05$) is probably not the most efficient one. Firstly,

it is possible to increase the lattice spacing somewhat, without substantial loss in accuracy. For example, going from $a=1$ to $a=2$ reduces the computational effort by a factor of 8. This increase seems, however, to be slightly too large already; as outlined in Sec. IV B, $a=2$ produces less accurate data. Secondly, one can try to exploit Eq. 3 by varying τ or a while keeping $\nu=2.8$, such that the simulation runs at $\lambda=-1$, for which the LBM algorithm takes a particularly simple form in which a substantial number of operations can be saved.[29] Further speedup can be expected if the requirement $\nu=2.8$ and $D_0=0.076$ (for mapping to MD) were released. However, we have not checked these questions in a systematic fashion; in particular, our discussion has not taken into account that the limit of stable time steps τ depends on both a and λ in a nontrivial way. We hence want to simply state that our present choice of parameters is not yet a fully optimized one; therefore the numbers given below (for $a=1$ and $\tau=0.05$) should be viewed as a lower bound of the efficiency which the method can attain.

On one EV5.6 processor of a 433 MHz DEC Alpha server 8400 (for a typical box size of $L=40$) our code obtains 3.1×10^5 grid point updates per second. In order to compare this number with the molecular-dynamics system, we note that one grid point corresponds to 0.86 solvent particles for $\rho=0.86$ and $a=1.0$. Therefore, the efficiency of the code in MD units is $3.1\times10^5\times0.86\approx2.7\times10^5$ particle updates per second. This number should be contrasted with the efficiency of optimized MD codes for short-range LJ fluids, which is[48] (on the same machine) 2.1×10^5 particle updates per second, using the code described in Ref. 49. Thus, the LBM would run by a factor of 1.3 faster than MD if the same time step were used. However, the lattice Boltzmann time step $\tau=0.05$ is more than an order of magnitude larger than for the pure MD system: The latter must be run without friction and noise, i.e., in the microcanonical ensemble, in order to strictly conserve momentum (otherwise the hydrodynamic interaction would be screened[50]). Such a simulation can only be stable on long time scales if the time step is sufficiently small; according to our experiences,[44] one needs $\Delta t=0.003$. Taking these factors into account, we obtain a net speedup of a factor of 22, which, as outlined above, can be increased further by choosing a coarser lattice, i.e., by trading in accuracy for speed. A detailed comparison with the "competitor" DPD[17–23] is highly desirable, but not done here, last but not least because the match of the viscosity is much less trivial in DPD.[21,22] From what we know from the literature, we expect that the two methods would be roughly comparable in speed, at least by order of magnitude.

B. Static and dynamic behavior

In order to check how well the new method produces the same physics as the original MD model,[7] from which all simulation parameters were derived, we focus on the comparison of the structure factor $S(k,t)$ for both methods, as shown in Fig. 9 (time dependence at constant k), Fig. 10 (k dependence at constant time), and Fig. 11 (time dependence for the *normalized* structure factor).

Let us first consider the *static* case $t=0$. The corresponding plot (Fig. 10, uppermost part) for $N_{ch}=30$ shows
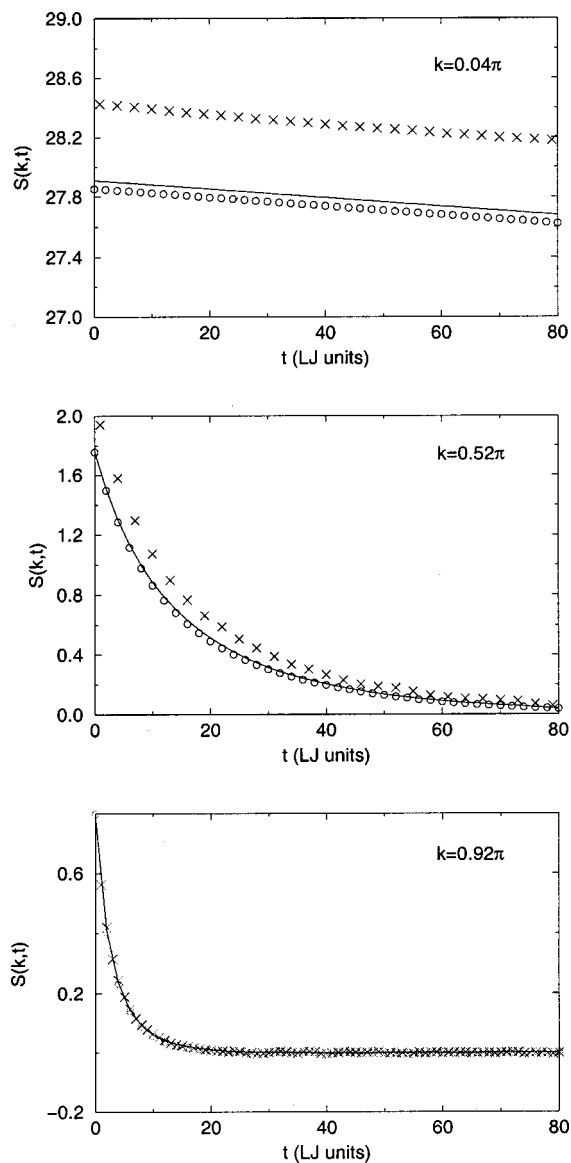
FIG. 9. The dynamic structure factor $S(k,t)$ for the new method with $\tau = 0.05$ (circles) and $\tau = 0.01$ (line) compared to pure MD simulation (crosses) for three different k values ($N_{ch} = 30$).
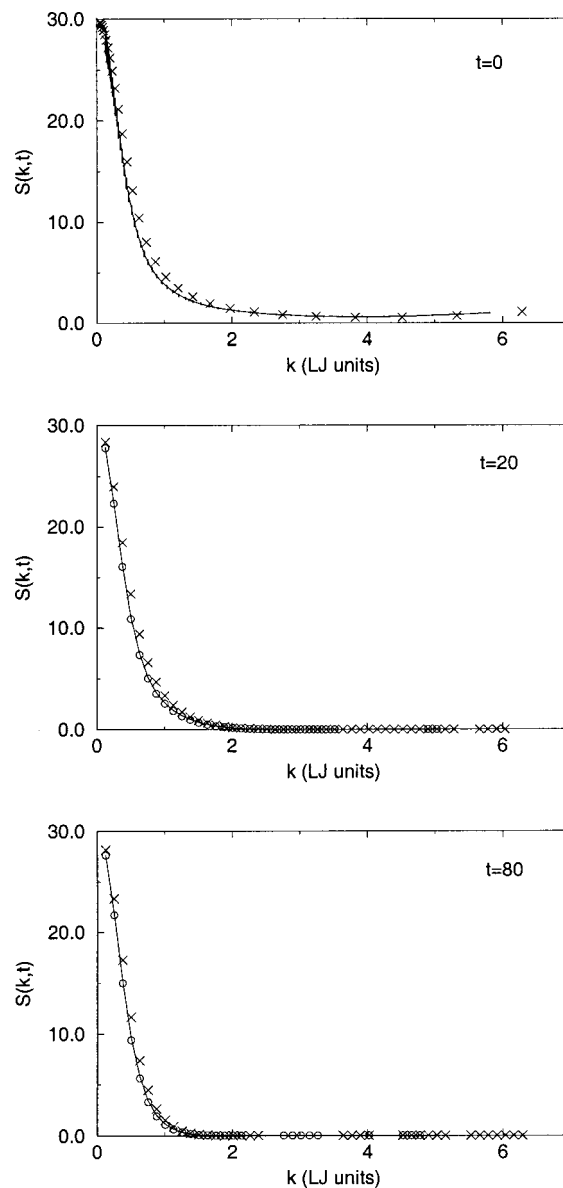

FIG. 10. The dynamic structure factor $S(k,t)$ for the new method with $\tau = 0.05$ (circles) and $\tau = 0.01$ (line) compared to pure MD simulation (crosses) for three different times ($N_{ch} = 30$).

systematic deviations. These manifest for example in the discrepancies of the static scaling exponent ($\nu = 0.59$ for the pure MD simulation, $\nu = 0.62 \ldots 0.64$ for the new method); the chain is more stretched using the new method. The absolute values for the static structure factor differ up to about 25%. Similar results hold if one compares other static quantities like the radius of gyration or the end–to–end distance. It can be verified that the discrepancies show no significant dependency on the chain length for the range investigated here (30–60). Moreover, they are not due to a discretization error in time, as the plots for $\tau = 0.05$ and $\tau = 0.01$ show. The reason is rather simply the fact that the MD chain is subject to a different potential (intrachain plus solvent) than the LBM chain (intra–chain only). For that reason, there is a systematic difference in the static conformations, which then, in turn, will also affect the dynamic properties somewhat. For example, the $N_{ch} = 60$ chain has a gyration radius $\langle R_g^2 \rangle^{1/2} = 5.79$, while the corresponding MD chain[7] has a gy-

ration radius of only 4.78. It is hence not surprising that the larger chain is also somewhat slower, as the comparison of the diffusion constants confirms ($D_{CM} = 3.39 \times 10^{-3}$ for the larger LBM chain, and $D_{CM} = 4.25 \times 10^{-3}$ for the smaller MD chain). Therefore, in order to achieve a better match of static and dynamic properties, it would be necessary to re–adjust the potential for the LBM chain such that the conformations are more similar. This is possible, but not completely trivial, and has not been attempted in this work. On the other hand, for the dynamics parameters (i.e., the viscosity and the friction coefficient), it is quite easy to achieve matching, as has been described in Sec. III A.

Turning to the decay of $S(k,t)$, we first note that the direct comparison of the data (Figs. 9 and 10) yields similar discrepancies of up to 25% as for the static case. The overall agreement is however quite reasonable. In order to divide out the trivial amplitude effect, we also plot $S(k,t)/S(k,0)$ for
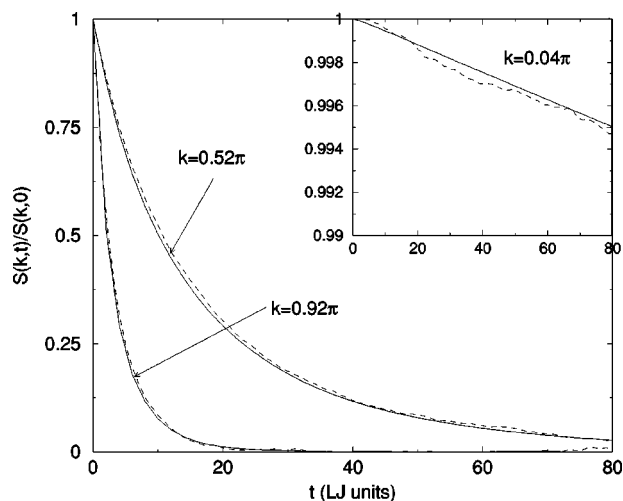
FIG. 11. $S(k,t)/S(k,0)$ for $N_{ch}=60$ using the new method (solid lines) with $\tau=0.05$ compared to pure MD simulation (dashed lines) for three different k values.

FIG. 12. Comparison of $S(k,t)/S(k,0)$ for $N_{ch}=30$, two different lattice spacings, and three k values as indicated.

three different k values in Fig. 11. For k in the scaling regime, the agreement is much better, with differences of a few percent only. This is not too surprising, since in this regime the decay rate should in essence be given by $k^3 k_B T/\eta$ times a numerical prefactor which depends only weakly on the details of the chain statistics.[46,47] In the long–wavelength regime (inset of Fig. 11) the decay is given by $\exp(-D_{CM}k^2 t)$, which is nicely confirmed by the data, and thus the ratio of the decay rates is just the ratio of the diffusion constants, i.e., there is again a discrepancy of roughly 20% (this is hardly visible in Fig. 11, due to noise in the MD data).

To summarize, we find that both methods are well-suited for quantitatively reproducing the dynamics of polymer chains in solvent, and both reveal Zimm behavior very nicely. The discrepancies which we find in the dynamic properties can be directly traced back to the nonperfect match of the static conformations. If those had been matched by an adjustment of the potential, then the agreement would probably be close to perfect.

Finally, let us discuss in more quantitative terms the influence of the lattice spacing. To this end, Fig. 12 compares the decay of the normalized dynamic structure factor of an $N_{ch}=30$ chain for three k values, obtained by running the same system with two different lattice spacings $a=1$ (as discussed previously) and $a=2$. All other simulation parameters (in particular the box volume, and the monomeric diffusion coefficient D_0—*not* the bare coupling ζ_{bare}) were left identical. As one sees from the figure, the larger lattice spacing induces decays which are systematically slower, by roughly 20%–25%. It is thus a question of desired accuracy if one wants to consider these results as still acceptable or not. The observed effect goes in the direction which one expects, for the following reasons: As soon as the lattice spacing exceeds the size of the chain, there will be no hydrodynamics left and one will observe pure Rouse dynamics, which is slower. Of course, this must be a systematic crossover as a function of lattice spacing. Thus one expects a decrease of the hydrodynamic correlations with increasing a
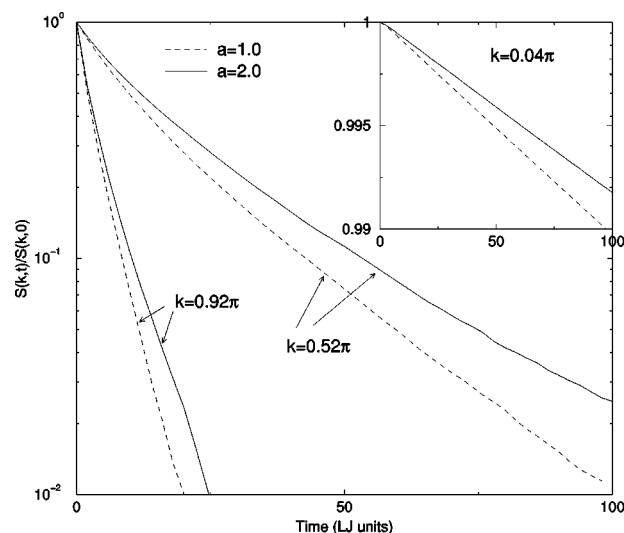
(also consistent with the reasoning at the end of Sec. II C), and hence a systematic slowdown of the dynamics.

V. CONCLUSION AND OUTLOOK

With this paper we have established a new method to simulate polymer–solvent systems. The solvent is modeled by the lattice Boltzmann method and the polymer by a continuum bead–spring model. The two parts are coupled using a simple dissipative friction ansatz which locally conserves mass and momentum. The driving force of the system are thermal fluctuations which are added to both the fluid and the polymer. The main advantage of the new method compared to MD is its computational efficiency, which amounts to a factor of 20, or even more, if one is willing to be satisfied with less accurate results.

As described in Sec. III A, it is possible to obtain the physical input parameters for the new method from results of existing MD simulations. Therefore, one can view the present method as a coarse-graining procedure where one goes in a well-controlled way from small length and time scales to larger ones. As the results show, this is possible without substantial loss of information about the statics and dynamics on the mesoscopic scale.

The input which is needed from a more microscopic approach consists of: (i) Effective potentials for the coarse–grained monomers such that the static chain conformations are roughly reproduced (this was the part to which we did not pay much attention, with the result that this is the largest source for the observed deviations); (ii) the solvent temperature, density and viscosity, and (iii) the monomeric diffusion coefficient, from which one adjusts the coupling.

It seems that a lattice spacing which roughly matches the chain's bond length and the interparticle distance of the solvent is optimal. A lattice constant which is chosen too large will result in underestimated hydrodynamic interactions, as seen from the data with $a=2$, while a too small lattice spacing will result in a large computational effort, plus (if it

J. Chem. Phys., Vol. 111, No. 17, 1 November 1999

Simulation of a single polymer chain   8237

becomes very small) a monomeric diffusion coefficient which will exceed any realistic value, due to an effective Stokes radius which is too small.

We have chosen the parameters of Ref. 7 for our simulation and performed a detailed quantitative comparison of the results. The main deviations result from insufficient match of the static conformations. The current model is, therefore, as appropriate as the original MD model for verification of Zimm dynamics in dilute polymer solutions. The dynamic scaling laws (in particular the $k^3 t$ decay of the dynamic structure factor) could be observed, and there is good agreement with the decay rates predicted by the Zimm model, if the finite box size effects are taken into account. Interestingly enough, the decay of the Rouse modes is only subject to an L^{-3} finite size effect, while most other decay rates have a large L^{-1} finite size correction, due to the r^{-1} behavior of the Oseen tensor.

After having tested the method successfully future work can now deal with more controversial problems, like the influence of hydrodynamics on the motion of a semiflexible chain or the hydrodynamic screening in semidilute solutions. It should however be kept in mind that the algorithm in its current version is only suitable for problems where the polymer concentration is low. The coupling only takes into account the momentum transfer between monomers and solvent. Excluded–volume effects between solvent particles and monomers, which are very important for processes like, e.g., the penetration of solvent into a dense polymer matrix, are not properly modeled. A study of such topics would require a generalization of the algorithm which would assign a finite volume to the monomers.

ACKNOWLEDGMENTS

APPENDIX A: INITIAL DECAY RATE OF ROUSE MODES

In this appendix we outline the details of the calculation of Γ_p, i.e., the initial decay rate of the autocorrelation function of the Rouse modes for $p \geq 1$, where we treat the general case of a chain whose statistics is described by an exponent ν [i.e., $\nu = 0.5$ for a random walk (RW), and $\nu = 0.6$ for a self–avoiding walk (SAW)]. We start by stating the result of linear response theory,[3]

$$\Gamma_p = -\frac{d}{dt}\left(\frac{\langle \mathbf{X}_p(t)\mathbf{X}_p(0)\rangle}{\langle \mathbf{X}_p^2 \rangle}\right)\Bigg|_{t=0}$$

$$= \frac{1}{\langle \mathbf{X}_p^2 \rangle} \sum_{i,j,\alpha,\beta,\gamma} \left\langle \frac{\partial X_{p\gamma}}{\partial r_{i\alpha}} D_{ij\alpha\beta} \frac{\partial X_{p\gamma}}{\partial r_{j\beta}} \right\rangle, \quad (A1)$$

where Greek indices again denote Cartesian coordinates. Evaluating the derivatives of the Rouse modes, one obtains

$$\Gamma_p = \frac{1}{\langle \mathbf{X}_p^2 \rangle N_{ch}^2} \sum_{i,j} \cos\left(\frac{p\pi}{N_{ch}}(i-1/2)\right)$$

$$\times \cos\left(\frac{p\pi}{N_{ch}}(j-1/2)\right) \text{Tr}\langle \mathbf{D}_{ij}\rangle. \quad (A2)$$

From the definition of the Rouse modes, Eq. (37), one finds

$$\langle \mathbf{X}_p^2 \rangle = \frac{1}{N_{ch}^2} \sum_{ij} \langle \mathbf{r}_i \cdot \mathbf{r}_j \rangle \cos\left(\frac{p\pi}{N_{ch}}(i-1/2)\right)$$

$$\times \cos\left(\frac{p\pi}{N_{ch}}(j-1/2)\right), \quad (A3)$$

which is evaluated via (b is the bond length)

$$\mathbf{r}_i \cdot \mathbf{r}_j = \frac{1}{2}[\mathbf{r}_i^2 + \mathbf{r}_j^2 - (\mathbf{r}_i - \mathbf{r}_j)^2], \quad (A4)$$

$$0 = \sum_{i=1}^{N_{ch}} \cos\left(\frac{p\pi}{N_{ch}}(i-1/2)\right), \quad (A5)$$

$$\langle (\mathbf{r}_i - \mathbf{r}_j)^2 \rangle = b^2 |i-j|^{2\nu}, \quad (A6)$$

(note that the last relation holds only asymptotically for large $|i-j|$). Approximation by an integral yields

$$\langle \mathbf{X}_p^2 \rangle = -\frac{b^2}{2N_{ch}^2} \int_0^{N_{ch}} dx \int_0^{N_{ch}} dy |x-y|^{2\nu}$$

$$\times \cos\left(\frac{p\pi}{N_{ch}}x\right)\cos\left(\frac{p\pi}{N_{ch}}y\right). \quad (A7)$$

Furthermore, we use the relation

$$\cos\alpha\cos\beta = \tfrac{1}{2}[\cos(\alpha-\beta)+\cos(\alpha+\beta)], \quad (A8)$$

and transform to the variables

$$u = \frac{p\pi}{N_{ch}}(x-y), \quad v = \frac{p\pi}{N_{ch}}(x+y). \quad (A9)$$

Exploiting the symmetry of the integrand with respect to u, and performing the integration over v, we find

$$\langle \mathbf{X}_p^2 \rangle = \frac{b^2 N_{ch}^{2\nu}}{2(p\pi)^{1+2\nu}} f(p), \quad (A10)$$

with

$$f(p) = \frac{1}{p\pi} \int_0^{p\pi} du \, u^{2\nu}[\sin u - (p\pi - u)\cos u]. \quad (A11)$$

For the RW case, $f(p)$ is exactly unity, while for the SAW case a weak dependence on p remains; however, also in this case $f(p)$ is close to one. Using the MAPLE software package, we have numerically evaluated this function; for the first 20 Rouse modes it is tabulated in Table II.

The calculation of the numerator of Eq. (A2) is performed using precisely the same procedure, the only difference being that $\langle (\mathbf{r}_i - \mathbf{r}_j)^2 \rangle$ is replaced by $\text{Tr}\langle \mathbf{D}_{ij}\rangle$, which we calculate using the finite box size form, Eq. (28)

TABLE II. The functions $f(p)$, $h(p)$, and $r(p)$, as defined in the text, for both the RW and the SAW case.

	RW	SAW		
p	$h(p)=r(p)$	$f(p)$	$h(p)$	$r(p)$
1	1.040 901	1.229 939	1.531 335	1.245 049
2	1.155 368	1.096 321	1.671 897	1.525 007
3	1.186 325	1.099 453	1.711 021	1.556 248
4	1.203 640	1.075 431	1.732 468	1.610 952
5	1.213 328	1.077 224	1.744 639	1.619 569
6	1.220 118	1.067 140	1.753 074	1.642 778
7	1.224 789	1.068 286	1.758 929	1.646 496
8	1.228 399	1.062 691	1.763 420	1.659 391
9	1.231 138	1.063 494	1.766 850	1.661 363
10	1.233 376	1.059 915	1.769 636	1.669 601
11	1.235 174	1.060 514	1.771 886	1.670 781
12	1.236 696	1.058 018	1.773 782	1.676 515
13	1.237 967	1.058 484	1.775 371	1.677 278
14	1.239 069	1.056 638	1.776 745	1.681 508
15	1.240 014	1.057 013	1.777 926	1.682 029
16	1.240 849	1.055 589	1.778 967	1.685 283
17	1.241 579	1.055 899	1.779 880	1.685 654
18	1.242 234	1.054 765	1.780 696	1.688 239
19	1.242 815	1.055 026	1.781 422	1.688 510
20	1.243 341	1.054 101	1.782 079	1.690 615

$$\text{Tr}\langle \mathbf{D}_{ij}\rangle = \frac{k_BT}{\eta\pi^2}\int_{k_0}^{\infty}dk\langle\exp(i\mathbf{k}\cdot\mathbf{r}_{ij})\rangle, \tag{A12}$$

where we have replaced the summation over wave numbers by an integral

$$\frac{1}{L^3}\sum_{\mathbf{k}\neq 0} \rightarrow \frac{1}{(2\pi)^3}\int_{k_0}^{\infty}4\pi k^2 dk, \tag{A13}$$

$k_0 = 2\pi/L$ denoting the cutoff wavenumber due to the finite box size.

The factor $\langle\exp(i\mathbf{k}\cdot\mathbf{r}_{ij})\rangle$ describes the structure of the chain, and must, for reasons of scaling,[1] asymptotically have the form

$$\langle\exp(i\mathbf{k}\cdot\mathbf{r}_{ij})\rangle = g(k^2b^2|i-j|^{2\nu}). \tag{A14}$$

It should be noted that, for reasons of inflection symmetry, g must depend on k^2, and that $g(0)=1$. We further introduce the constants

$$A = \int_0^{\infty}dw\, g(w^2), \tag{A15}$$

$$B = \left.\frac{dg(w^2)}{dw^2}\right|_{w=0}. \tag{A16}$$

For example, for a random walk one has $g = \exp(-(b^2/6)k^2|i-j|)$, i.e., $g(w^2)=\exp(-w^2/6)$, $A = \sqrt{3\pi}/2$, $B = -1/6$. We now calculate $\text{Tr}\langle\mathbf{D}_{ij}\rangle$ by performing a Taylor expansion with respect to $k_0 = O(L^{-1})$; the result is

$$\text{Tr}\langle\mathbf{D}_{ij}\rangle = \frac{k_BT}{\eta\pi^2}\left[\frac{A}{b|i-j|^{\nu}}-k_0-\frac{B}{3}b^2|i-j|^{2\nu}k_0^3\right]$$
$$+O(k_0^5). \tag{A17}$$

Interestingly, the linear term does not depend on the monomer indices at all. From this, we conclude that the linear L^{-1} contribution to the decay rate exactly vanishes, due to Eq. (A5), and that the leading order finite size effect is actually of order L^{-3}, i.e., quite small. In what follows we will, therefore, only concentrate on the leading–order term for an infinite box. Using the same procedure as for $\langle\mathbf{X}_p^2\rangle$, one finds

$$\int_0^{N_{\text{ch}}}dx\int_0^{N_{\text{ch}}}dy\frac{1}{|x-y|^{\nu}}\cos\left(\frac{p\pi}{N_{\text{ch}}}x\right)\cos\left(\frac{p\pi}{N_{\text{ch}}}y\right)$$
$$= \frac{N_{\text{ch}}^{2-\nu}}{(p\pi)^{1-\nu}}h(p), \tag{A18}$$

with

$$h(p) = \frac{1}{p\pi}\int_0^{p\pi}du\frac{1}{u^{\nu}}[(p\pi-u)\cos u - \sin u]. \tag{A19}$$

This function also exhibits a weak p-dependence, see Table II, even for a RW. Finally, introducing

$$r(p) = h(p)/f(p), \tag{A20}$$

also tabulated in Table II, we can write the result for Γ_p as

$$\Gamma_p = A\frac{2}{\pi^2}\frac{k_BT}{\eta b^3}\left(\frac{p\pi}{N_{\text{ch}}}\right)^{3\nu}r(p). \tag{A21}$$

The leading power–law dependence on p and N_{ch} is exactly what one expects from dynamic scaling. The function $r(p)$ is a correction to scaling. As far as the numerical prefactor is concerned, we get (in the RW case) a relaxation which is roughly the same as that calculated in the textbook by Doi and Edwards.[3]

[1] P.-G. deGennes, *Scaling Concepts in Polymer Physics* (Cornell, Ithaca, 1979).
[2] G. Strobl, *The Physics of Polymers*, 2nd ed. (Springer, Berlin, 1997).
[3] M. Doi and S. F. Edwards, *The Theory of Polymer Dynamics* (Clarendon, Oxford, 1986).
[4] *Monte Carlo and Molecular Dynamics Simulation in Polymer Science*, edited by K. Binder (Clarendon, Oxford, 1995).
[5] B. Dünweg, G. S. Grest, and K. Kremer, in *Numerical Methods for Polymeric Systems*, edited by S. G. Whittington (Springer, Berlin, 1998), IMA Volumes in Mathematics and its Applications 102, p. 159.
[6] K. Kremer and G. S. Grest, J. Chem. Phys. **92**, 5057 (1990).
[7] B. Dünweg and K. Kremer, J. Chem. Phys. **99**, 6983 (1993).
[8] C. Pierleoni and J.-P. Ryckaert, J. Chem. Phys. **96**, 8539 (1992).
[9] W. Smith and D. C. Rapaport, Mol. Simul. **9**, 25 (1992).
[10] J. G. Kirkwood and J. Riseman, J. Chem. Phys. **16**, 565 (1948).
[11] J. P. Erpenbeck and J. G. Kirkwood, J. Chem. Phys. **29**, 909 (1958).
[12] B. H. Zimm, J. Chem. Phys. **24**, 269 (1956).
[13] D. L. Ermak and J. A. McCammon, J. Chem. Phys. **69**, 1352 (1978).
[14] J. F. Brady and G. Bossis, Annu. Rev. Fluid Mech. **20**, 111 (1988).
[15] W. Zylka and H. C. Öttinger, J. Chem. Phys. **90**, 474 (1989).
[16] A. Rey, J. J. Freire, and J. G. de la Torre, Macromolecules **24**, 4666 (1991).
[17] P. J. Hoogerbrugge and J. M. V. A. Koelman, Europhys. Lett. **19**, 155 (1992).
[18] A. G. Schlijper, P. J. Hoogerbrugge, and C. W. Manke, J. Rheol. **39**, 567 (1995).
[19] R. D. Groot and P. B. Warren, J. Chem. Phys. **107**, 4423 (1997).
[20] P. Español and P. B. Warren, Europhys. Lett. **30**, 191 (1995).
[21] C. Marsh, G. Backx, and M. H. Ernst, Europhys. Lett. **38**, 411 (1997).
[22] P. Español, Phys. Rev. E **57**, 2930 (1998).
[23] I. Pagonabarraga, M. H. J. Hagen, and D. Frenkel, Europhys. Lett. **42**, 377 (1998).

[24] P. Ahlrichs and B. Dünweg, Int. J. Mod. Phys. C **9**, 1429 (1998).

[25] R. Benzi, S. Succi, and M. Vergassola, Phys. Rep. **222**, 145 (1992).

[26] S. Chen and G. D. Doolen, Annu. Rev. Fluid Mech. **30**, 329 (1998).

[27] A. J. C. Ladd, J. Fluid Mech. **271**, 311 (1994).

[28] D. O. Martínez, W. H. Matthaeus, S. Chen, and D. C. Montgomery, Phys. Fluids **6**, 1285 (1994).

[29] A. J. C. Ladd, J. Fluid Mech. **271**, 285 (1994).

[30] L. D. Landau and E. M. Lifshitz, *Fluid Mechanics* (Addison-Wesley, Reading, 1959).

[31] P. L. Bhatnagar, E. P. Gross, and M. Krook, Phys. Rev. **94**, 511 (1954).

[32] J. O. Hirschfelder, C. F. Curtiss, and R. B. Bird, *Molecular Theory of Gases and Liquids*, 2nd ed. (Wiley, New York, 1964).

[33] A. J. Wagner, Europhys. Lett. **44**, 144 (1998).

[34] Y. H. Qian, D. D'Humières, and P. Lallemand, Europhys. Lett. **17**, 479 (1992).

[35] D. Frenkel and B. Smit, *Understanding Molecular Simulation* (Academic, San Diego, 1996).

[36] W. Kalthoff, S. Schwarzer, G. Ristow, and H. J. Herrmann, Int. J. Mod. Phys. C **7**, 543 (1996).

[37] N. S. Martys, X. Shan, and H. Chen, Phys. Rev. E **58**, 6855 (1998).

[38] Y. Oono and K. F. Freed, J. Chem. Phys. **75**, 1009 (1981).

[39] A. D. Sokal, in *Monte Carlo and Molecular Dynamics Simulation in Polymer Science*, edited by K. Binder (Clarendon, Oxford, 1995), Chap. 2.

[40] C. W. J. Beenakker, J. Chem. Phys. **85**, 1581 (1986).

[41] M. Fixman, Macromolecules **14**, 1710 (1981).

[42] M. Fixman, J. Chem. Phys. **78**, 1594 (1983).

[43] J. Batoulis and K. Kremer, Macromolecules **22**, 4277 (1989).

[44] A. Kopf, B. Künweg, and W. Paul, J. Chem. Phys. **107**, 6945 (1997).

[45] P.-G. deGennes, Physics **3**, 37 (1967).

[46] A. Z. Akcasu, M. Benmouna, and C. C. Han, Polymer **21**, 866 (1980).

[47] M. Benmouna and A. Z. Akcasu, Macromolecules **13**, 409 (1980).

[48] T. Soddemann, private communication (unpublished).

[49] M. Pütz and A. Kolb, Comput. Phys. Commun. **113**, 145 (1998).

[50] B. Dünweg, J. Chem. Phys. **99**, 6977 (1993).